

Graph Neural Network-Based Anomaly Detection for River Network Systems

Katie Buchhorn^{1,2}, Edgar Santos-Fernandez^{1,2}, Kerrie Mengersen^{1,2}, and Robert Salomone^{1,3}

¹Queensland University of Technology, School of Mathematical Sciences

²Queensland University of Technology, Centre for Data Science

³Queensland University of Technology, School of Computer Science

Abstract

Water is the lifeblood of river networks, and its quality plays a crucial role in sustaining both aquatic ecosystems and human societies. Anomaly detection is crucial for identifying erroneous patterns in sensor data, but can be a challenging task due to the complexity and variability of the data, even under normal conditions. This paper presents a solution to the challenging task of anomaly detection for river network sensor data, which is essential for the accurate and continuous monitoring of water quality. We use a graph neural network model, the recently proposed Graph Deviation Network (GDN), which employs graph attention-based forecasting to capture the complex spatio-temporal relationships between sensors. We propose an alternate anomaly threshold criteria for the model, GDN+, based on the learned graph. To evaluate the model's efficacy, we introduce new benchmarking simulation experiments with highly-sophisticated dependency structures and subsequence anomalies of various types. We further examine the strengths and weaknesses of this baseline approach, GDN, in comparison to other benchmarking methods on complex real-world river network data. Findings suggest that GDN+ outperforms the baseline approach in high-dimensional data, while also providing improved interpretability. We also introduce software called `gnnad`.

Keywords

Anomaly Detection, Graph Deviation Network, Graph Neural Network, Multivariate Time Series, Graph Attention Forecasting, Spatio-temporal Data, Complex Systems

Introduction

River network systems play a vital role as freshwater habitats for aquatic life, and as support for terrestrial ecosystems in riparian zones, but are particularly sensitive to the anthropogenic impacts of climate change, water pollution and over-exploitation, among other factors. As a United Nations Sustainable Development Goal [1], water quality is a major environmental concern worldwide. The use of *in-situ* sensors for data collection on river networks is increasingly prevalent, generating large amounts of data that allow for the identification of fine-scale spatial and temporal patterns, trends, and extremes, as well as potential sources of pollutants and their downstream impacts. However, such sensors are susceptible to technical errors relating to the equipment, herein defined as *anomalies*, for example due to miscalibration, biofouling, electrical interference and battery failure. In contrast, extreme events in rivers occur as result of heavy rain and floods. Technical anomalies must be identified before the data is considered for further analysis, as they can introduce bias in model parameters and affect the validity of statistical inferences, which then confounds the identification of true changes in water variables. Trustworthy data is needed to produce reliable and accurate assessments of water quality, for enhanced environmental monitoring, and for guiding management decisions in the prioritisation of ecosystem health.

Anomaly detection in river networks is challenging due to the highly dynamic nature of river water even under typical conditions [2], as well as the complex spatial relationships between sensors. The unique spatial relationships between neighbouring sensors on a river network are characterised by a branching network topology with flow direction and connectivity, embedded within the 3-D terrestrial landscape. Common anomalies from data obtained from *in-situ* sensors are generally characterised by multiple consecutive observations (subsequence or persistent), including sensor drift and periods of unusually high or low variability, which may indicate the necessity for sensor maintenance or calibration [3]. Such anomalies are difficult to detect and often associated with high false negative rates [4].

Earlier statistical studies have focused on developing autocovariance models based on within-river relationships to capture the unique spatial characteristics of rivers [5]. Although these methods are adaptable to different climate zones, and have recently been extended to take temporal dependencies into account [6], data sets generated by *in-situ* sensors still pose significant computational challenges with such prediction methods due to the sheer volume of data [7]. Autocovariance matrices must be inverted when fitting spatio-temporal models and making predictions and this can be a challenge for high-frequency dataset. Previous work [8], evaluated several neural networks for detecting drift and high-variability anomalies in water quality variables, calibrated using a Bayesian multi-objective optimization procedure. However, the study was limited to analyzing univariate time series data, and the supervised methods required a significant amount of

labeled data for training, which are not always available.

There are limited unsupervised anomaly detection methods for subsequence anomalies (of variable length), and even less so for multivariate time series anomaly detection [9]. One such method uses dynamic clustering on learned segmented windows to identify global and local anomalies [10]. However, this algorithm requires the time series to be well-aligned, and is not suitable for the lagged temporal relationships observed with river flow. Another method to detect variable-length subsequence anomalies in multivariate time series data uses dimensionality reduction to construct a one-dimensional feature, to represent the density of a local region in the recurrence representation, indicating the recurrence of patterns obtained by a sliding window [11]. A similarity measure is used to classify subsequences as either non-anomalous or anomalous. Only two summary statistics were used in this similarity measure and the results were limited to a low-dimensional simulation study. In contrast, the technique introduced by [12], DeepAnT, uses a deep convolutional neural network (CNN) to predict one step ahead. This approach uses Euclidean distance of the forecast errors as the anomaly score. However, an anomaly threshold parameter must be provided.

Despite the above initial advances, challenges still remain in detecting persistent variable-length anomalies within high-dimensional data exhibiting noisy and complex spatial and temporal dependencies. With the aim of addressing such challenges, we explore the application of the recently-proposed Graph Deviation Network (GDN) [13], and explore refinements with respect to anomaly scoring that specifically address the needs of environmental monitoring. The GDN approach [13] is a state-of-the-art model that uses sensor embeddings to capture inter-sensor relationships as a learned graph, and employs graph attention-based forecasting to predict future sensor behaviour. Anomalies are flagged when the error scores are above a calculated threshold value. By learning the interdependencies among variables and predicting based on the typical patterns of the system, this approach is able to detect deviations when the expected spatial dependencies are disrupted. As such, GDN offers the ability to detect even the small-deviation anomalies generally overlooked by other distance based and density based anomaly detection methods for time series, while offering robustness to lagged variable relationships. Unlike the commonly-used statistical methods that explicitly model covariance as a function of distance, GDN is flexible in capturing complex variable relationships independent of distance. GDN is also a semi-supervised approach, eliminating the need to label large amounts of data, and offers a computationally efficient solution to handle the ever increasing supply of sensor data. Despite the existing suite of methods developed for anomaly detection, only a limited number of corresponding open-source software is available to practitioners. In summary, we have identified the following gaps in the current literature and research on this topic:

1. An urgent need exists for a flexible approach that can

effectively capture complex spatial relationships in river networks without the specification of an auto-covariance model, and the ability to learn from limited labeled data.

2. Lack of data and anomaly generation schemes on which to benchmark methods, that exhibit complex spatial and temporal dependencies, as observed across river networks.
3. Lack of open-source software for anomaly detection, which hinders the accessibility and reproducibility of research in this field, and limits the ability for individuals and organizations with limited resources to implement effective anomaly detection strategies.

Our work makes four primary contributions to the field:

1. An improvement of the GDN approach via the threshold calculation based on the learned graph is presented, and shown to detect anomalies more accurately than GDN while improving the ability to locate anomalies across a network.
2. New simulation data generation methods for highly-sophisticated spatio-temporal structures, contaminated with various types of persistent anomalies are provided as benchmarking data.
3. Experimentation on benchmark data, as well as a real-world river network dataset, is conducted to evaluate the strengths and limitations of GDN (and its variants) in increasingly challenging settings.
4. User-friendly, free open-source software for the GDN/GDN+ approach is available on the pip repository as `gnnad`, with data and anomaly generation modules.

The structure of the remaining paper is as follows: the next section details the methods of GDN, and the model extension GDN+, and describes the methodology of the simulated data and anomaly generation. In the Results section we present an extensive simulation study on the benchmarking data, and a real-world case study. In each case, the performance of GDN/GDN+ is assessed against other state-of-the-art anomaly detection models. Further details and example code for the newly-released software is also provided. The paper concludes with a discussion of the findings, and the strengths and weaknesses of this model.

Methods

Consider multivariate time series data $\mathbf{Y} = [\mathbf{y}^{(1)}, \dots, \mathbf{y}^{(T)}]$, obtained from n sensors over T time ticks. The (univariate) data collected from sensor $i = 1, \dots, n$ at time $t = 1, \dots, T$ is denoted as $y_i^{(t)}$. Following the standard semi-supervised anomaly detection approach [14, 15], non-anomalous data is used for training, while the test set may contain anomalous data. That is, we aim to learn the sensor behaviour using data obtained under standard operational conditions throughout the

training phase and identify anomalous sensor readings during testing, as those which deviate significantly from the learned behaviour. As the algorithm output, each test point $\mathbf{y}^{(t)}$ is assigned a binary label, $a(t) \in \{0, 1\}$, where $a(t) = 1$ indicates an anomaly at time t , anywhere across the full sensor network.

The GDN approach for anomaly detection is composed of two aspects:

1. **Forecasting-based time series model:** a non-linear autoregressive multivariate time series model that involves graph neural networks is trained, and
2. **Threshold-based anomaly detection:** transformations of the individual forecasting errors are used to determine if an anomaly as occurred, if such errors exceed a calculated threshold.

The above components are described individually below.

Forecasting-based Time Series Model. To predict $\mathbf{y}^{(t)}$, the model takes as input $p \in \mathbb{N}$ lags of the multivariate series,

$$\mathbf{X}^{(t)} := [\mathbf{y}^{(t-1)}, \dots, \mathbf{y}^{(t-p)}].$$

The i -th row (containing sensor i 's measurements for the previous p lags) of the above input matrix is denoted by $\mathbf{x}_i^{(t)} \in \mathbb{R}^p$, represented as a column vector. Prior to training, the practitioner specifies acceptable *candidate relationships* via the sets $\mathcal{C}_1, \dots, \mathcal{C}_n$, where each $\mathcal{C}_i \subseteq \{1, 2, \dots, n\}$ and does not contain i . These sets specify which nodes are allowed to be considered to be connected from node i (note the adjacency graph connections are not necessarily symmetric).

The model implicitly learns a graph structure via training *sensor embedding* parameters $\mathbf{v}_i \in \mathbb{R}^d$ for $i = 1, \dots, n$ which are used to construct a graph. The intuition is that the embedding vectors capture the inherent characteristics of each sensor, and that sensors which are “similar” in terms of the angle between their vector embeddings are considered connected. Formally, the quantity e_{ji} is defined as the cosine similarity between the vector embeddings of sensors i and j :

$$e_{ji} = \frac{\mathbf{v}_i^\top \mathbf{v}_j}{\|\mathbf{v}_i\| \|\mathbf{v}_j\|} \mathbb{I}\{j \in \mathcal{C}_i\}, \quad i, j \in \{1, \dots, n\},$$

with $\|\cdot\|$ denoting the Euclidean norm, and indicator function \mathbb{I} which equals 1 when node j belongs to set \mathcal{C}_i , and 0 otherwise. Note that the similarity is forced to be zero if a connecting node is not in the permissible candidate set. Next, write $e_{j,(i)}$ for the i -th largest value in (e_{j1}, \dots, e_{jn}) . A *graph-adjacency matrix* (and in turn a graph itself) is then constructed from the sensor similarities via:

$$A_{ji} = \mathbb{I}\{\{e_{ji} \geq e_{j,(K)}\} \cup \{i = j\}\},$$

for user-specified $K \in \{1, \dots, n\}$ which determines the maximum number of edges from a node, referred to as the “Top-K” hyperparameter.

The above describes how the trainable parameters $\{\mathbf{v}_k\}_{k=1}^n$ yield a graph. Next, the lagged series are fed

individually through a shallow *Graph Attention Network* [16] that uses the previously constructed graph. Here, each *node* corresponds to a sensor, and the *node features* for node i are the lagged (univariate) time-series values $\mathbf{x}_i^{(t)} = (y_i^{(t-1)}, \dots, y_i^{(t-p)})$. Allow parameter weight matrix $\mathbf{W} \in \mathbb{R}^{d \times p}$ to apply a shared linear transform to each node. Then, the output of the network is given by

$$\mathbf{z}_i^{(t)} = \max \left\{ \mathbf{0}, \left(\sum_{j: A_{ji} > 0} \alpha_{ij} \mathbf{W} \mathbf{x}_j^{(t)} \right) \right\},$$

where $\mathbf{z}_i^{(t)}$ is called the *node representation*, and coefficients α_{ij} are the attention paid to node j when computing the representation for node i , with:

$$\pi_{ij} = \text{LeakyReLU} \left(\mathbf{a}^\top (\mathbf{v}_i \oplus \mathbf{W} \mathbf{x}_i^{(t)} + \mathbf{v}_j \oplus \mathbf{W} \mathbf{x}_j^{(t)}) \right), \quad (1)$$

$$\text{where } \alpha_{ij} = \frac{\exp(\pi_{ij})}{\sum_{k: A_{ki} > 0} \exp(\pi_{ik})}.$$

with learnable parameters $\mathbf{a} \in \mathbb{R}^{2d}$, where \oplus denotes concatenation, and $\text{LeakyReLU}(\mathbf{x}) := \max\{\delta \mathbf{x}, \mathbf{x}\}$ for $\delta > 0$, with the maximum operation applied elementwise. Note the addition¹ in Equation (1) and that $\sum_{j=1}^n \alpha_{ij} = 1$. Intuitively, the above is an automated mechanism to aggregate information from a node itself and neighbouring nodes (whilst simultaneously assigning a weight of how much information to take from each neighbour) to compute a vector representing extracted information about node i itself and its neighbours' interaction with it. The final model output (prediction) is given by,

$$\hat{\mathbf{y}}^{(t)} = f_\eta \left([\mathbf{v}_1 \odot \mathbf{z}_1^{(t)}, \dots, \mathbf{v}_n \odot \mathbf{z}_n^{(t)}] \right),$$

where $f_\eta : \mathbb{R}^{d \times n} \rightarrow \mathbb{R}^n$ is a feedforward neural network with parameters η , and \odot denotes element-wise multiplication. The model is trained via optimizing the parameters $\{\mathbf{v}_i\}_{i=1}^n$, \mathbf{W} , \mathbf{a} , and η to minimize the *mean squared error* loss function

$$\mathcal{L} = \frac{1}{N-p} \sum_{t=p+1}^N \left\| \hat{\mathbf{y}}^{(t)} - \mathbf{y}^{(t)} \right\|^2.$$

Threshold-based Anomaly Detection. Given the learned inter-sensor and temporal relationships, we are able to detect anomalies as those which deviate from these interdependencies. An *anomalousness score* is computed for each time point in the test data. For each sensor i , define univariate vector of prediction errors as,

$$\epsilon_i = |\mathbf{y}_i^{(t)} - \hat{\mathbf{y}}_i^{(t)}|.$$

Note that $\epsilon_i \in \mathbb{R}^{N-p}$. Since the error values of different sensors may vary significantly, we perform a robust normalisation of each sensor's errors to prevent any one sensor from overly dominating the others, that is,

$$\tilde{\epsilon}_i = \left(\frac{\epsilon_i - \text{Median}(\epsilon_i)}{\text{IQR}(\epsilon_i)} \right),$$

¹It seems that the authors of [13] mistakenly denote this addition as concatenation in the paper, however, their corresponding reference code computes addition.

where IQR denotes *inter-quartile range*. In the original work by [13], a time point t is flagged as anomalous if,

$$A(t) = \mathbb{I}\{\max_i(\tilde{\epsilon}_{i,t}) > \kappa\},$$

using the notation $\tilde{\epsilon}_{i,t}$ for the error value at the t -th index. Alternatively, the authors recommend using a *simple moving average* of $\tilde{\epsilon}_i$ and flagging time t as anomalous if the maximum of that moving average exceeds κ . The authors specify κ as the maximum of the normalised errors observed on some (non-anomalous) validation data, denoted by variant epsilon, $\tilde{\epsilon}$. However, this is applied to all sensors as a fixed threshold.

The behavior of water quality variables may differ across space, for example, water level at high-altitude river network branches are generally characterised by rainfall patterns, whereas water level downstream near a river outlet can also be influenced by tidal patterns. A fixed threshold across the network does not allow for any local adaptations in error sensitivity. For this reason, this work also considers the novel sensor-specific threshold calculation,

$$A_i(t) = \mathbb{I}\{\tilde{\epsilon}_{i,t} > \kappa_i\},$$

where κ_i is chosen such that,

$$\frac{1}{|\{\tilde{\epsilon}_{j,t}\}_{j: A_{ji} > 0}|} \sum_{j: A_{ji} > 0} \mathbb{I}\{\tilde{\epsilon}_{j,t} < \kappa_i\} = \tau,$$

for some user-specified quantile, $\tau \in (0, 1)$, and where $|\cdot|$ is the cardinality. In other words, the threshold for each sensor, κ_i , is set as the τ -th quantile of the normalised error scores across the neighbourhood of i , on the validation data set. Unless otherwise stated, set $\tau = 0.99$. In this way, the sensor threshold is based only on its direct neighbourhood, as opposed to the original method which uses the global maximum, and is thus more robust as a percentile and in tune with the local behaviour of the system. We refer to the GDN model using this variant of the threshold-based anomaly detection as GDN+.

New Class of Benchmarking Data

The following is a method for simulating synthetic datasets with persistent anomalies inspired by the statistical models commonly used to model river network data [6]. Let \mathcal{S} denote an arbitrary set of individual spatial locations, with locations $\mathbf{s}_1, \mathbf{s}_2, \dots, \mathbf{s}_n \in \mathcal{S}$ chosen by experimental design [17] or otherwise. Consider a linear mixed model with $n \times 1$ response \mathbf{Y} , and $n \times m$ design matrix \mathbf{X} of explanatory variables spatially indexed at locations $\mathbf{s}_1, \mathbf{s}_2, \dots, \mathbf{s}_n$,

$$\mathbf{Y}_t = \boldsymbol{\beta}_0 + \mathbf{X}_t \boldsymbol{\beta} + \mathbf{Z} + \boldsymbol{\epsilon}_0, \quad t = 1, \dots, T, \quad (2)$$

with time-homogeneous spatially-correlated random effects $\mathbf{Z} \sim \mathcal{N}(\mathbf{0}, \boldsymbol{\Sigma}_Z)$ and vector of independent noise terms $\boldsymbol{\epsilon}_0 \sim \mathcal{N}(\mathbf{0}, \sigma_0^2 \mathbf{I})$, yielding $\text{Cov}[\mathbf{Y}_t | \mathbf{X}_t = \mathbf{x}_t] = \boldsymbol{\Sigma}_Z + \sigma_0^2 \mathbf{I}$, where \mathbf{I} denotes the $n \times n$ identity matrix and $\boldsymbol{\epsilon}_0$ is an error term. The covariates \mathbf{X}_t for $t = 1, \dots, T$ are simulated according to an autoregressive process based on an underlying sequence of independent random fields,

$$\mathbf{X}_t = \sum_{i=0}^p \varphi_i \tilde{\mathbf{X}}_{t-i},$$

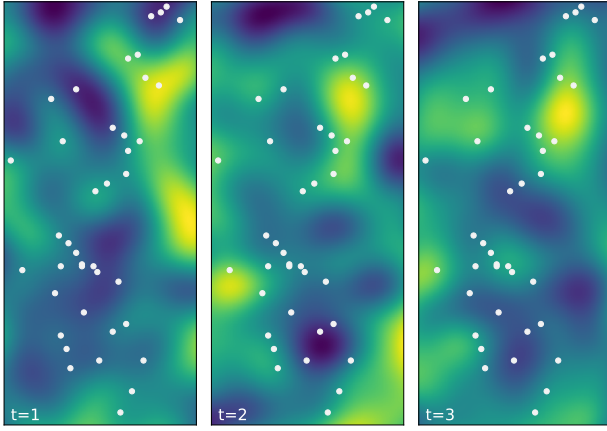


Figure 1. Smooth random Gaussian field used to generate covariate values, X , in the simulation studies. Examples of the field are shown for $t = 1, 2, 3$. Sensor locations are shown as white dots.

where p is the order of the autoregressive process, and

$$\tilde{X}_t \stackrel{\text{iid}}{\sim} \mathcal{N}(\mathbf{0}, \Sigma_X), \quad t = 1, \dots, T.$$

Above,

$$(\Sigma_X)_{ij} = k(s_i, s'_j)$$

for some covariance kernel k . For example,

$$k(s, s'; \sigma, \alpha) = \sigma^2 \exp\left(-\frac{\|s - s'\|^2}{\alpha}\right), \quad (3)$$

where $\|\cdot\|$ denotes the Euclidean norm, $\sigma^2 > 0$ is the covariance-scaling parameter, and $\alpha \in \mathbb{R}$ is the range parameter that controls the rate of decay of correlation between points over distance. Figure 1 illustrates an example of a generated Gaussian random field evolving over time.

We consider two scenarios in generating the covariance matrix Σ_Z : 1) spatial relationships characterised by Euclidean distance only, and 2) data simulated on a river network, see Figure 2. Two points s_i, s_j on a river network are said to be *flow-connected* if they share water flow, and *flow-unconnected* otherwise. We define stream distance, $h_{\text{Riv}}(s_i, s_j)$, as the shortest distance separating s_i and s_j when travelling *along* a given river network. Tail-up covariance models for river networks, introduced in [5], effectively represent spatial relationships when variables are dominated by flow (e.g. pollutants enter a stream and only impact downstream locations). By construction, the tail-up covariance function only allows for correlation between flow-connected sites:

$$k_{\text{TU}}(s_i, s_j; \sigma, \alpha) = \omega_{ij} \sigma^2 \exp\left(-\frac{h_{\text{Riv}}(s_i, s_j)}{\alpha}\right) \mathcal{F}_{ij}, \quad (4)$$

where \mathcal{F}_{ij} is equal to one if s_i and s_j are flow-connected, and zero otherwise, and ω_{ij} is a weighting attributed to each stream segment to account for the upstream branching network structure and ensure stationarity in variance

(for full details, see [18, 19]). The weightings corresponding to each segment may incorporate flow volume, or the area of the catchment, or a proxy such as stream order [20]. Note that there are various choices of models for decay [5], we use the exponential model.

In the first case, the covariance matrix, Σ_Z , is constructed via the kernel function given in Equation (3), and in the second case, via the kernel function given in Equation (4). Together, this approach provides a variety of simulated data with highly-sophisticated dependency structure.

Once the base multivariate time series is constructed as above, it is modified to include river-network type anomalies as follows. Hyperparameters are, $n_{\text{anomalies}} \in \mathbb{R}$, the number of subsequence anomalies, p_{anomaly} , the probability assigned to each anomaly type and, $\lambda_{\text{anomaly}} > 0$, the average length of an anomalous subsequence. In this example, we consider two types of anomalies, high-variability and drift, see Algorithm 1.

Algorithm 1: Two-type Anomaly Generation

input : Time series data $Y = [y^{(1)}, \dots, y^{(T)}]$, locations $s_1, s_2, \dots, s_n \in \mathcal{S}$, proportion of each anomaly type, $p_{\text{anomaly}} \in (0, 1)$, expected length of each anomaly type, λ_{anomaly} , and the total instances of anomalies, $n_{\text{anomalies}}$.

for $i = 1, \dots, n_{\text{anomalies}}$ **do**

- Draw location $S \sim \text{Uniform}(\{1, 2, \dots, n\})$
- Draw time $t \sim \text{Uniform}(\{1, \dots, T\})$
- if** $U(0, 1) < p_{\text{drift}}$ **then**
 - Draw $L \sim \text{Poisson}(\lambda_{\text{drift}})$ // anomaly length
 - $v \leftarrow (\alpha, 2\alpha, \dots, L\alpha)$ // drift
- else**
 - Draw $L \sim \text{Poisson}(\lambda_{\text{variability}})$
 - $v \sim \mathcal{N}(\mathbf{0}, \sigma^2 I_{L \times L})$ // variability
- $y_{S, t:(t+L)} \leftarrow y_{S, t:(t+L)} + v$

Results

This section presents a summary of the main findings for anomaly detection using GDN/GDN+ on both simulated and real-world data. To ensure quality of data, the aim for practitioners is to maximise the ability to identify anomalies of different types, while minimising false detection rates. We define the following metrics in terms of true positive (TP), true negative (TN), false positive (FP) and false negative (FN) classifications. In other words, the main priority is to minimise FN, while maintaining a reasonable number of FP, such that it is not an operational burden to check the total number of positive flags. Accordingly, we use recall, defined by $\frac{\text{TP}}{\text{TP} + \text{FN}}$, to evaluate the performance on the test set and to select hyperparameters. That is, the proportion of actual positive cases that were correctly identified by the model(s). We also report the performance using precision ($\frac{\text{TP}}{\text{TP} + \text{FP}}$), accuracy ($\frac{\text{TP} + \text{TN}}{\text{TP} + \text{TN} + \text{FP} + \text{FN}}$) and specificity ($\frac{\text{TN}}{\text{TN} + \text{FP}}$).

To evaluate model performance, three existing anomaly detection models are used as benchmarks: 1. The naive (random walk) Autoregressive Integrated Moving Average Model (ARIMA) prediction model from [21, 4]; 2.

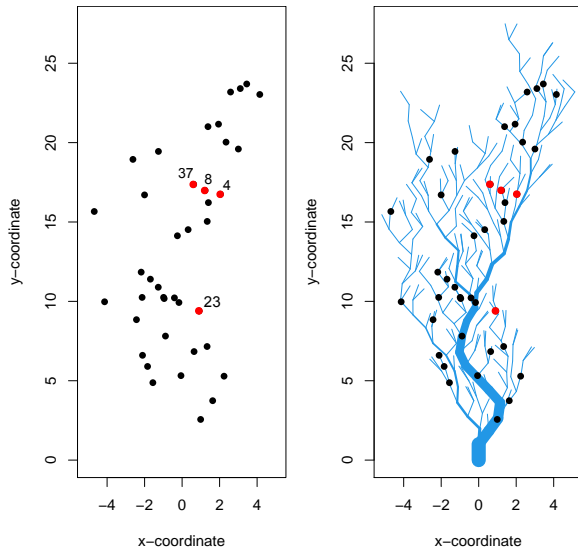


Figure 2. SimEuc site locations across space (left) and SimRiver site locations along a river network (right). Both simulations use the same (x, y) coordinates for sensor locations. The direction of flow is from top to bottom for SimRiver. Red dots indicate sites for which time series have been shown in Figure 3 and Figure 4.

HDoutliers [22], an unsupervised algorithm designed to identify anomalies in high-dimensional data, based on a distributional model that allows for probability assignment to an anomaly; and 3. DeepAnT [12], an unsupervised, deep learning-based approach to detecting anomalies in time series data.

Simulation Study: Benchmark data

Data are generated using the linear-mixed model described in Equation (2), with differing spatial dynamics: *SimEuc* where the random effect, Z , is characterised by Euclidean distance only, and *SimRiver* where Z simulates complex river network dynamics, using the same site locations and covariate values, X (see accompanying code for details). Detecting anomalies involving multiple consecutive observations remains a difficult task and often requires user intervention, since they affect the spatio-temporal structure, and is the focus of this example. We consider scenarios with drift and high-variability anomaly types, which together contaminate 13.2% of the test data, see Table 1.

Table 1. Details of the three data sets used in the case studies.

Dataset	#Train	#Test	%Anomalies
SimEuc	3,000	1,000	13.2
SimRiver	3,000	1,000	13.2
Herbert	12,745	3,499	58.0

Figure 3 visualises aspects of the SimEuc dataset, where sensor 37 and sensor 8 are in close (Euclidean) proximity, resulting in a high correlation between the locations

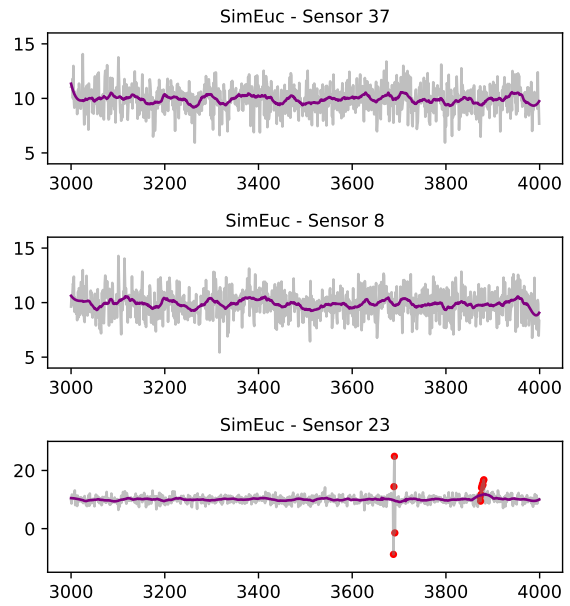


Figure 3. A selection of time series from the SimEuc data set; sensor 8 and sensor 37 separated by a short Euclidean distance share high correlation (coefficient of 0.65). A Savitzky-Golay filter smoothes the time series (purple line). On the bottom, sensor 23 illustrates high-variability and drift anomalies, consecutively (red dots).

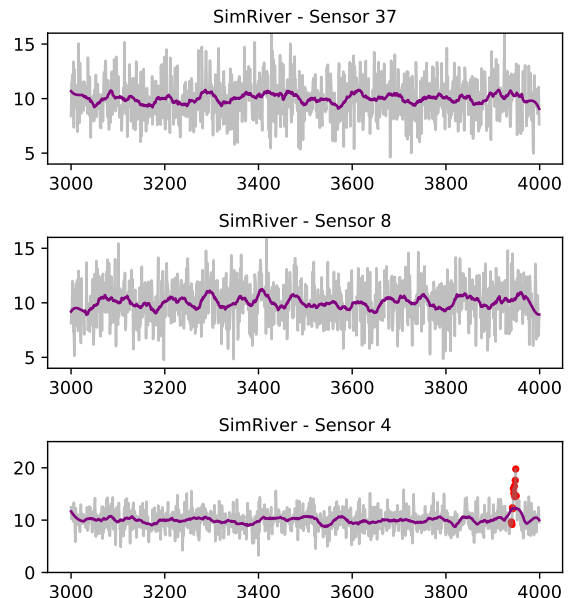


Figure 4. A selection of series from the SimRiver data set; sensor 8 and sensor 37 are not flow-connected sites, and share low correlation (coefficient of 0.07). Drift anomalies (red dots) are shown in data from sensor 4. A Savitzky-Golay filter is used to smoothen the time series for visual representation (purple line).

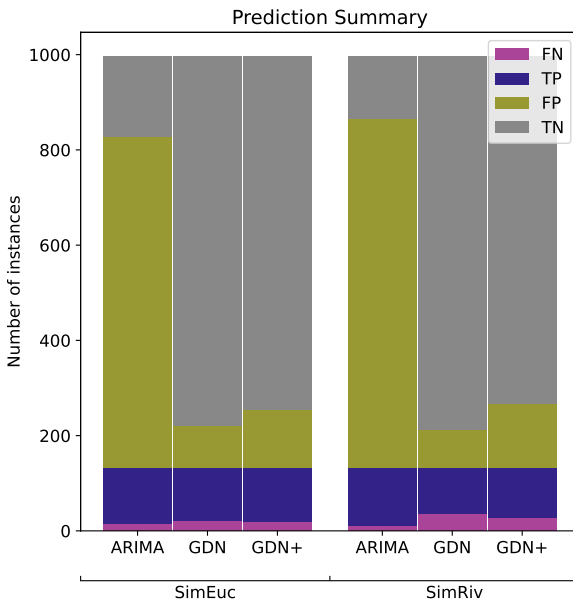


Figure 5. Anomaly detection performance of ARIMA, GDN, and GDN+ for the simulation study, in terms of true positive (TP), true negative (TN), false positive (FP) and false negative (FN).

(0.65), as anticipated. Note that sensor 23 exhibits anomalous behavior, high-variability and drift, consecutively, over time. Compared to the SimRiver dataset, shown in Figure 4, we note how the time series from sensor 37 and sensor 8 are no longer strongly correlated (0.07), despite their close proximity, as they are not flow-connected in the simulated river network.

Table 2 shows the performance of the different anomaly detection methods. The best performance in terms of recall is highlighted in bold, while the second-best performance is underlined. We observe that GDN/GDN+ outperformed most other models in terms of recall, which is the fraction of true positives among all actual positive instances. Specifically, GDN has a recall score of 83.3% on SimEuc and 72.7% on SimRiv, while GDN+ has the second highest recall score of 85.6% on SimEuc and 78.0% on SimRiv. Although ARIMA performed best in terms of recall, the high percentage of detected anomalies, 81.6% and 85.6%, is impractical to use (discussed below) and results in low accuracy scores of 28.6% and 25.3%, respectively. HDoutliers did not flag any time point as anomalous in any test case. DeepAnT tends to classify most samples as negative, resulting in a low recall score. These results suggest that GDN and its variants are best able to detect a high proportion of actual anomalies in the datasets. Figure 5 shows the classifications of anomalies in the simulation study in terms of true positive (TP), true negative (TN), false positive (FP) and false negative (FN). For reasons mentioned, recall is the performance metric of interest, but we also consider the trade-off between recall and precision. Lower precision means that the model may also identify some normal instances as anomalies, leading to false positives. In the context of river network anomaly

detection, FP may be manually filtered, but it is critical to minimise FN. Note that GDN+ improves in comparison to GDN in minimising the FN count, but at the cost of increasing FP, in both data sets. Such a trade-off is acceptable and considered an improvement. However, while ARIMA has the highest recall score, the number of FP is impractical for practitioners. We also note that drift anomalies are harder to detect than high-variability anomalies, with drift as the majority of FN counts, in all cases.

The authors of the GDN model demonstrated its efficacy in detecting anywhere-within-system failures at time t by applying a threshold to all sensors within a system. However, the use of sensor-based thresholds in GDN+ has the advantage of indicating anomalies at the individual sensor level. In the context of monitoring river networks, it is crucial to identify the anomalous sensor, i , at a given time t . The percentage of true positives detected at the correct sensor, i , using the sensor-based anomaly threshold, $A_i(t)$, in GDN+, was 92% and 89% for SimEuc and SimRiver, respectively. Similarly, the rate of true positives detected in the neighbourhood of the correct sensor i were 96% and 91%, respectively. This granularity of information is essential for large networks consisting of independent sensors that are separated by significant spatial distances, where the cost of time and travel for sensor replacement or maintenance is substantial.

Table 2. Anomaly detection performance in terms of recall (%), precision (%), accuracy (%), and specificity (%) of GDN and its variants and baseline methods.

Data	Model	Rec	Prec	Acc	Spec
SimEuc	HDoutliers	0.0	0.0	86.8	100.0
	ARIMA	88.6	14.4	28.6	19.4
	DeepAnT	3.8	11.9	83.5	95.7
	GDN	83.3	55.3	88.9	89.7
	GDN+	<u>85.6</u>	48.1	85.9	85.9
SimRiv	HDoutliers	0.0	0.0	86.8	100.0
	ARIMA	91.7	14.2	25.3	15.1
	DeepAnT	0.8	9.1	85.9	98.8
	GDN	72.7	54.2	88.3	90.6
	GDN+	<u>78.0</u>	43.1	83.5	84.3
Herbert	HDoutliers	0.0	0.0	42.0	100.0
	ARIMA	30.5	62.9	51.3	77.5
	DeepAnT	1.6	39.7	44.0	97.0
	GDN	29.2	60.6	50.1	76.2
	GDN+	<u>34.8</u>	59.2	50.4	70.0
	GDN++	100.0	80.7	86.7	70.0

Case Study: Herbert River

This case study examines water-level data collected from eight sites located across the Herbert river, a major river system located in the tropical region of Australia, as

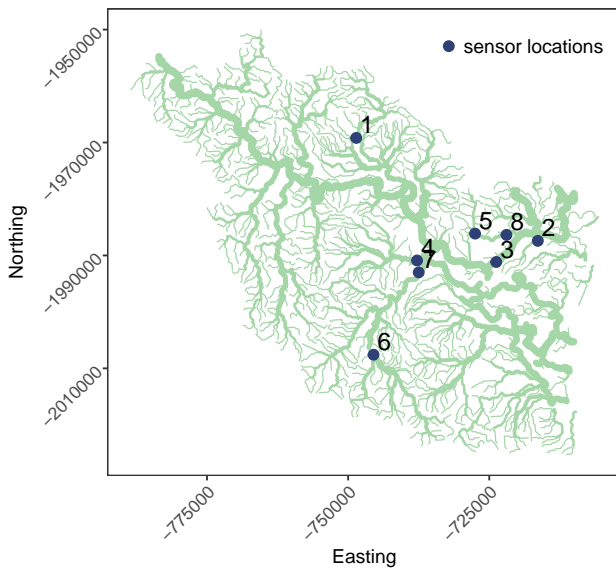


Figure 6. The Herbert river system and sensor locations.

shown in Figure 6. The time series data is highly non-stationary, characterised by river *events* caused by abnormal rainfall patterns, with some coastal sites exhibiting shorter periodicity trends which can be attributed to tidal patterns, see Figure 7. The spatial relationships are complex, and depend on the surrounding water catchment areas, spatial rainfall patterns, dams, and other impediments. In-situ sensors are prone to various anomalies such as battery failure, biofouling (accumulation of microorganisms, plants, algae, or small animals), and damage. In some cases, anomalies can manifest as the absence of a water event (i.e., flatlining) rather than the presence of abnormal time series patterns (i.e., spikes, variability, drift). In real-world scenarios, anomalies can persist for extended periods, and resolving them may require traveling to remote locations to inspect and repair sensors. As seen in Figure 7, anomalies at time t are largely attributed to Sensor 4, which was out of water for long periods of time.

The Herbert river is a challenging data set for all of the anomaly detection models, due to the sparse placement of sensors across the network, i.e., fewer sensors at greater distances apart resulting in weaker spatial relationships, and the test set contains a high proportion of anomalies (58%; see Table 1). GDN applied to the real-world dataset yields a recall of 29.2%, with GDN+ improving recall to 34.8%. Model performance suffers primarily due to the failure to detect the large anomaly spanning across 22-01-10 in Figure 7. This may be attributed to the learned graph relationships being characterised by river events in the training data, and without such events, it is difficult to identify when a sensor is flat-lining. However, the model successfully identified anomalies spanning across 2021-12-27 and 22-01-03, which coincided with river events.

Figure 8 shows the learned graph adjacency matrix, A .

Sensor 1, separated geographically by a large distance from the other sensors, has weaker relationships with the other nodes. Interestingly, the attention weights indicate that sensor 3 is strongly influenced by sensor 6, with tidal patterns from sensor 6 being evident in the predictions of sensor 3. Large error scores indicating an anomaly spanning across 2021-12-27 are primarily observed in sensor 2, impacted by anomalous sensors 3 and 4, where the predicted values are low. However, due to the small network of sensors in this case study, it is difficult to determine which sensor the anomaly originated from, since the hyperparameter for the number of permissible neighbours was, $topk = 6$, which is almost the size of the network itself.

Adjusting the threshold in the GDN+ model can only enhance performance to a limited extent, since some anomalies may have insignificant error scores due to the underlying time series model. For instance, the anomaly spanning across 22-01-10 has negligible error scores because the prediction model was performing well and no river events had occurred, making it challenging to detect the anomaly in this particular scenario. Therefore, relying solely on the model may not be sufficient, and we recommend implementing some basic expert rules. We introduce another model variant GDN++, by applying a simple filter to the time series ensuring that all values are positive, used in conjunction with adjusting the threshold calculation (GDN+). That is, an anomaly at time, t , on sensor, i , is flagged if, $\max\{\mathbb{I}\{y_i^{(t)} < 0\}, A_i(t)\} = 1$. GDN++ successfully detects all anomalies.

Python package

The Python package `gnnad` introduced in this paper extends and generalises the research code originally implemented by [13]. The code is refactored to be modular and user-friendly, with a scikit-inspired interface, and extended to include visualisation, data and anomaly generation modules, and the GDN+ model extension. A continuous integration/continuous deployment (CI/CP) pipeline is established with unit testing to ensure that changes to the code are tested and deployed efficiently. Comprehensive documentation now accompanying the codebase enhances readability for future developers, facilitating maintenance, reuse, and modification. Furthermore, rigorous error handling is implemented to improve the software experience. The software developments have resulted in a more robust, user-friendly and easily distributable package that is available via <https://github.com/KatieBuc/gnnad> and the pip repository, `gnnad`. See below for example code that shows the process of fitting the GDN+ model.

```
from gnnad.graphanomaly import GNNAD
from gnnad.generate import GenerateGaussian,
... GenerateAnomaly

# generate sample data
gengauss = GenerateGaussian()
X = gengauss.generate()

# split train test
```

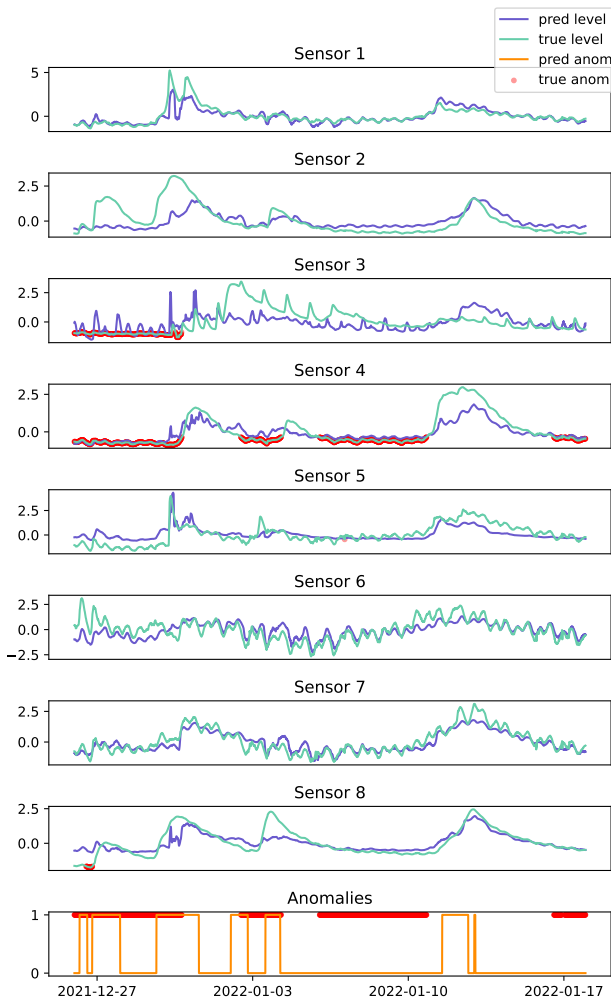


Figure 7. Test data of water level collected from sensors across the Herbert river (light blue), and the corresponding predictions from the GDN model (dark blue). Actual anomalies (red dots) are shown, along with the predicted anomalies (orange line) on the bottom.

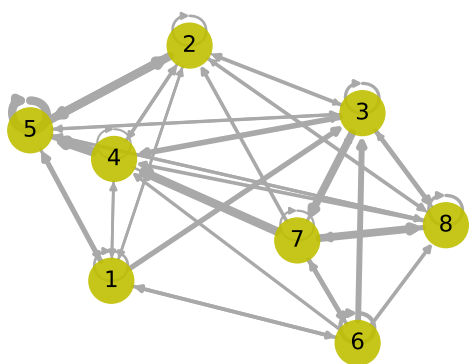


Figure 8. Graph with learned adjacency matrix, A . The edge weightings are determined by α_{ij} , which indicates attention and depend on model input, $X^{(t)}$.

```

X_train, X_test = X[:P,:], X[P:,:, :]
# generate anomalies on test set
anoms = GenerateAnomaly(X_test)
X_test = anoms.generate(anoms.variability,
... lam = 3, prop_anom = 0.07, seed=45)
X_test = anoms.generate(anoms.drift,
... lam = 11, prop_anom = 0.07, seed=234)
y_test = anoms.get_labels()

# instantiate and fit GDN model object
model = GNNAD(threshold_type="max_validation",
... topk=6, slide_win=200)
fitted_model = model.fit(X_train, X_test,
... y_test)

# sensor based threshold based on GDN+
pred_label = fitted_model.sensor_threshold_
... preds(tau = 99)

# print evaluation metrics
fitted_model.print_eval_metrics(pred_label)

```

Discussion

Multivariate anomaly detection and efficient prediction models for spatio-temporal sensor data have the potential to transform water quality observation, modelling, and management. The provision of trustworthy sensor data: 1. Enables the production of finer-scale, reliable and more accurate estimates of sediment and nutrient loads, 2. Provides real-time feedback to landholders and managers, 3. Guides compliance with water quality guidelines, and 4. Allows for the assessment of ecosystem health and the prioritisation of management actions for sustaining aquatic ecosystems. However, technical anomalies can occur due to factors such as low battery power, biofouling of the probes, and sensor miscalibration. As noted by [4], there are a wide variety of anomaly types present within in-situ sensor data (e.g., high-variability, drift, spikes, shifts). Most anomaly detection methods used for water quality applications tend to target specific anomalies, such as sudden spikes or shifts [23, 24, 25]. Detecting persistent anomalies, such as sensor drift and periods of abnormally high variability, remains very challenging for statistical and machine learning research. Such anomalies are often overlooked by distance and kernel based methods, yet must be detected before the data can be used, because they confound the assessment of status and trends in water quality. Understanding the relationships among, and typical behaviours of, water quality variables and how these differ among climate zones is thus an essential step in distinguishing anomalies from real water quality events.

We investigated the graph-based neural network model, GDN [13], for its ability to capture complex interdependencies between different variables in a semi-supervised manner. As such, GDN offered the ability to capture deviations from expected behaviour within a high-dimensional setting. We developed novel bench-marking data sets for subsequence anomaly detection (of variable length and

type), with a range of spatio-temporal complexities, inspired by the statistical models commonly used for river network data [6]. Results showed that GDN tended to outperform the benchmarks in anomaly detection. We developed a model extension, GDN+, by adjusting the threshold calculation that was shown to further improve performance. Sensor-based thresholds also proved useful in terms of identifying which neighbourhood the anomaly originated from.

We used a real-world case study of water level in the Herbert river, with non-stationary time series characterised by multiple river events caused by abnormal rainfall patterns. In this case, most of the anomalies arose due to the sensors being out-of-water. Considering an individual time series, such anomalies may not appear obvious, as it is the failure to detect river events (in a multivariate setting) that is indicative of an anomalous sensor. Despite the challenges in the data, GDN+ was shown to successfully detect technical anomalies when river events occurred, and combined with a simple expert-based rule, all anomalies were successfully detected. Future applications of this work could consider the separation of river events from technical anomalies. In terms of interpretability, since the prediction model aggregates feature data from neighbouring sensors, anomalous data can affect the prediction of any other sensor within the neighbourhood. Therefore, large error scores originating from one sensor anomaly can infiltrate through to the entire neighbourhood, and if the number of neighbours for each node is relatively high for the size of the network, the ability to identify from which sensor the anomaly originates suffers.

There are two recent methodological extensions to the GDN approach worth noting. First, the Fused Sparse Autoencoder and Graph Net [26] which extends the GDN approach by augmenting the prediction-based loss with a reconstruction-based term arising from the output of a sparse autoencoder, and a further extension that allows the individual sensors to have multivariate data. Second, a probabilistic (latent variable) extension is trained using variational inference [27].

In summary, this work extends and examines the practicality of the GDN approach when applied to an environmental monitoring application of major international concern, with complex spatial and temporal interdependences. Successfully addressing the challenge of anomaly detection in such settings can facilitate the wider adoption of in-situ sensors and could revolutionise the monitoring and management of air, soil, and water.

Conclusions

In this work, we used the Graph Deviation Network (GDN) approach for anomaly detection on river networks, high-dimensional data with complex spatio-temporal relationships. We introduce an extension of the model (GDN+) and assess the practicality of this approach on various data sets. Simulation studies showed that GDN was effective in accurately identifying anomalies, further improved by GDN+, with the improved ability to locate

anomalies across a network. Experiments on a real-world data set indicated that GDN, and its variants, are most effective in capturing river network dynamics when compared to other methods, but challenges still remain for anomaly detection on river network sensor data.

Author contributions

KB; Investigation, Formal Analysis, Methodology, Software, Validation, Visualization, Writing – Original Draft Preparation. RS; Methodology, Supervision, Writing – Review & Editing. KM; Funding Acquisition, Conceptualization, Methodology, Supervision, Writing – Review & Editing. ES; Data Curation, Visualization, Writing – Review & Editing.

Grant information

This work was supported by the Australian Research Council (ARC) Linkage Project (LP180101151) titled “Revolutionising water-quality monitoring in the information age” assigned to Kerrie Mengersen. Data are provided by the Department of Environment and Science, Queensland.

Acknowledgements

Łukasz Mentel; Software. James McGree; Writing – Review & Editing.

References

- [1] UN General Assembly Transforming our World: The 2030 Agenda for Sustainable Development. *United Nations*, (A/RES/70/1), 2015.
- [2] James M Kang, Shashi Shekhar, Michael Henjum, Paige J Novak, and William A Arnold. Discovering teleconnected flow anomalies: A relationship analysis of dynamic neighborhoods (RAD) approach. In *International Symposium on Advances in Spatial and Temporal Databases*, pages 44–61. Springer, 2009.
- [3] Wilfrid Bourgeois, Anne-Claude Romain, Jacques Nicolas, and Richard M Stuetz. The use of sensor arrays for environmental monitoring: interests and limitations. *Journal of Environmental Monitoring*, 5(6):852–860, 2003.
- [4] Catherine Leigh, Omar Alsibai, Rob J Hyndman, Sevvandi Kandanaarachchi, Olivia C King, James M McGree, Catherine Neelamraju, Jennifer Strauss, Priyanga Dilini Talagala, Ryan DR Turner, et al. A framework for automated anomaly detection in high frequency water-quality data from in situ sensors. *Science of the Total Environment*, 664: 885–898, 2019.
- [5] Jay M Ver Hoef and Erin E Peterson. A moving average approach for spatial statistical models of stream networks. *Journal of the American Statistical Association*, 105(489): 6–18, 2010.
- [6] Edgar Santos-Fernandez, Jay M Ver Hoef, Erin E Peterson, James McGree, Daniel J Isaak, and Kerrie Mengersen. Bayesian spatio-temporal models for stream networks. *Computational Statistics & Data Analysis*, 170:107446, 2022.

[7] John H Porter, Paul C Hanson, and Chau-Chin Lin. Staying afloat in the sensor data deluge. *Trends in Ecology & Evolution*, 27(2):121–129, 2012.

[8] Javier Rodriguez-Perez, Catherine Leigh, Benoit Liquet, Claire Kermorvant, Erin Peterson, Damien Sous, and Kerrie Mengersen. Detecting technical anomalies in high-frequency water-quality data using artificial neural networks. *Environmental Science & Technology*, 54(21):13719–13730, 2020.

[9] Ane Blázquez-García, Angel Conde, Usue Mori, and Jose A Lozano. A review on outlier/anomaly detection in time series data. *ACM Computing Surveys (CSUR)*, 54(3):1–33, 2021.

[10] Xing Wang, Jessica Lin, Nital Patel, and Martin Braun. Exact variable-length anomaly detection algorithm for univariate and multivariate time series. *Data Mining and Knowledge Discovery*, 32:1806–1844, 2018.

[11] Min Hu, Xiaowei Feng, Zhiwei Ji, Ke Yan, and Shengchen Zhou. A novel computational approach for discord search with local recurrence rates in multivariate time series. *Information Sciences*, 477:220–233, 2019.

[12] Mohsin Munir, Shoaib Ahmed Siddiqui, Andreas Dengel, and Sheraz Ahmed. DeepAnT: A deep learning approach for unsupervised anomaly detection in time series. *Ieee Access*, 7:1991–2005, 2018.

[13] Ailin Deng and Bryan Hooi. Graph neural network-based anomaly detection in multivariate time series. In *Proceedings of the AAAI Conference on Artificial Intelligence*, volume 35, pages 4027–4035, 2021.

[14] Markus Goldstein and Seiichi Uchida. A comparative evaluation of unsupervised anomaly detection algorithms for multivariate data. *PloS one*, 11(4):e0152173, 2016.

[15] Ali Bou Nassif, Manar Abu Talib, Qassim Nasir, and Fatima Mohamad Dakalbab. Machine learning for anomaly detection: A systematic review. *Ieee Access*, 9:78658–78700, 2021.

[16] Petar Velivcković, Guillem Cucurull, Arantxa Casanova, Adriana Romero, Pietro Lio, and Yoshua Bengio. Graph attention networks. *International Conference on Learning Representations (ICLR)*, 2018.

[17] Katie Buchhorn, Kerrie Mengersen, Edgar Santos-Fernandez, Erin E Peterson, and James M McGree. Bayesian design with sampling windows for complex spatial processes. *arXiv preprint arXiv:2206.05369*, 2022.

[18] Noel Cressie, Jesse Frey, Bronwyn Harch, and Mick Smith. Spatial prediction on a river network. *Journal of Agricultural, Biological, and Environmental Statistics*, 11(2):127, 2006.

[19] Jay M Ver Hoef, Erin Peterson, and David Theobald. Spatial statistical models that use flow and stream distance. *Environmental and Ecological Statistics*, 13(4):449–464, 2006.

[20] Ronald L Shreve. Statistical law of stream numbers. *The Journal of Geology*, 74(1):17–37, 1966.

[21] Rob J Hyndman and George Athanasopoulos. *Forecasting: principles and practice*. OTexts, third edition, 2021.

[22] Leland Wilkinson. Visualizing big data outliers through distributed aggregation. *IEEE transactions on visualization and computer graphics*, 24(1):256–266, 2017.

[23] Priyanga Dilini Talagala, Rob J Hyndman, Catherine Leigh, Kerrie Mengersen, and Kate Smith-Miles. A feature-based procedure for detecting technical outliers in water-quality data from in situ sensors. *Water Resources Research*, 55(11):8547–8568, 2019.

[24] David J Hill and Barbara S Minsker. Anomaly detection in streaming environmental sensor data: A data-driven modeling approach. *Environmental Modelling & Software*, 25(9):1014–1022, 2010.

[25] Amadou Ba and Sean A McKenna. Water quality monitoring with online change-point detection methods. *Journal of Hydroinformatics*, 17(1):7–19, 2015.

[26] Siho Han and Simon S Woo. Learning sparse latent graph representations for anomaly detection in multivariate time series. In *Proceedings of the 28th ACM SIGKDD Conference on Knowledge Discovery and Data Mining*, pages 2977–2986, 2022.

[27] Wenchao Chen, Long Tian, Bo Chen, Liang Dai, Zhibin Duan, and Mingyuan Zhou. Deep Variational Graph Convolutional Recurrent Network for Multivariate Time Series Anomaly Detection. In *International Conference on Machine Learning*, pages 3621–3633. PMLR, 2022.